2950 Niles Road, St. Joseph, MI 49085-9659, USA
269.429.0300 fax 269.429.3852 hq@asabe.org www.asabe.org

An ASABE Meeting Presentation
DOI: 10.13031/aim.20162460299
Paper Number: 162460299

Modeling Ground Penetrating Radar (GPR) Technology for Seed Planting Depth Detection using Numerical Scheme based on Finite Difference Time Domain (FDTD) Method

Kenneth O.M. Mapoka[1], Stuart J. Birrell[2], Tekeste Mehari[3]
Agricultural & Biosystems Engineering, Iowa State University, Ames, IA 50011[123]

Written for presentation at the
2016 ASABE Annual International Meeting
Sponsored by ASABE
Orlando, Florida
July 17-20, 2016

[Click here to mention other presentations of this paper (optional)]

(The ASABE disclaimer is in a table that will print at the bottom of this page. Delete this message.)

ABSTRACT. *Ground Penetrating Radar (GPR) is an electromagnetic (EM) signal based technology, commonly used as a non-destructive technique to explore subsurface features and identify different depth profiles in materials. The overall goals of this work is to evaluate GPR for non-destructive mapping of seed planting depth. Soils are inherently complex materials and numerous factors affect GPR behavior. The fundamental factors affecting GPR response are dielectric permittivity, magnetic permeability, and electrical conductivity, which are influenced by soil bulk density, texture, salinity, organic matter, volumetric water content, seed properties and physical geometry. To successfully optimize GPR's ability to detect seed planting depth, the influence of these factors must be evaluated. This paper describes the development of a single dimensional GPR simulation model, based on finite difference time domain (FDTD) method, to evaluate the use of GPR sensing of seed planting depth. The simulation results shows that the EM signal is highly sensitive to high values of the electrical conductivity. High permittivity values decrease the EM signal velocity, wavelength and strength. A combination of these two properties leads to a significant EM signal attenuation ranging from 0 to ~ 800 dBm-1 as the signal traverses through the soil and seed. The lack of sufficient dielectric contrast between soil and seed presents a challenge on the detectability of the reflected signal by the radar receiver, therefore a sufficient dielectric contrast between the soil and seed has to be present to allow the GPR to be a viable tool to map the seed planting depth.*

Keywords. *Conductivity, Electromagnetic, Finite Difference, Permittivity and Seed Planting Depth.*

Introduction

Planting depth is a critical aspect in crop production. Measures to control planting depth have been designed and developed. However, measures to detect the location and determining seed depths have not been developed. In this study the electromagnetic and dielectric properties of soils are investigated, to evaluate the potential for development of seed depth sensors. Since, soils are inherently heterogeneous, there is a challenge in trying to understand the effect of different soil parameters on sensor response. Therefore, isolation of the effects of the difference electromagnetic properties is extremely important in evaluating Ground Penetrating Radar (GPR) signal performance, using developed finite difference time domain (FDTD) simulation models. GPR is a technique used to provide high resolution imagery of the subsurface features, that is used across disciplines, including geology, archaeology, engineering, and agriculture. In agricultural applications, GPR technology has been used extensively to map spatial variability, classifying soils, and mapping drainage pipes on agricultural fields (Allred et al., 2005; Allred et al., 2004; Lameck, Robert, Ronald, & Hines, 2002; Yoder, Freeland, Ammons, & Leonard, 2001). The technique explicitly employs physical principles for evaluations of any geometrical system. Therefore, GPR can be defined as a geophysical technique, and commonly used as a nondestructive technology for subsurface exploration. In addition to high resolution imagery, GPR is capable of providing planimetric positions and depth of buried objects (Jol, 2009; Weia & Hashimb, 2012) by employing electromagnetic (EM) signals. GPR is indiscriminant on its detection algorithm which means metals and nonmetals can be equally detected, which makes the technology versatile across all discipline i.e. engineering, agriculture etc.

At the heart of the GPR technology exist EM signals. These EM signals are highly frequency dependent. At high frequencies, EM signals can penetrate a material surface at the speed of light without causing any harm to the host material. Principles of EM signals were founded by James Clerk Maxwell. Maxwell principles are captured in greater detail by (Jol 2009; Sadiku 2010). For electromagnetic signals to yield useful information, propagated signals need to be reflected and received back by the receiver and deciphered for interpretation. Reflected signals are function of electrical properties of the medium which the signal is traversing. EM signals traverses easily on a dielectric material. A dielectric material is characterized by three constitutive electrical properties: permittivity, permeability and electrical conductivity. These constitutive properties interact with EM signal from Maxwell's curl equations to map the subsurface.

Maxwell's equations are predominantly defined in their partial derivatives and integral functions. In this paper partial derivatives functions are used. These partial differentials represent the space-time dependent Maxwell's curl equation that can be successfully discretized in space and time using FDTD formulation. The FDTD computational analysis is termed volumetric. The computational analysis done by (Yee, 1966) solved the electric and magnetic fields volumetrically using a leapfrog principle. The premise of leapfrog in the time domain is based on: computing the electric field at an instant time and spatial volume while the magnetic field is computed at the next instant in time at the same spatial volume. The process is repetitive until a specified time period has elapsed. The author used a lattice with predefined cells to compute the progression of the fields in given space and time period. At each time step and spatial volume, the partial derivatives are approximated using the FDTD central differences evaluated at the center of each cell. The FDTD used in this paper is a distinctively explicit numerical method. Predictions of next field amplitude in time and space are based on known values of the previous time step. In this paper 1D FDTD model is implemented in Matlab. Matlab language is used because of its simplicity in coding the FDTD formulation and it features excellent graphic tools offering excellent visualization of the fields as they traverse through the problem space. Geometries are modeled using transverse electric fields (TE) and absorbing boundaries conditions are explicitly defined, to prevent reflections back into the computational space. FDTD is a commonly used numerical technique to solve Maxwell's curl equations, in that, it offers sufficient advantages compared to other numerical techniques such as the finite element method, method of moments etc., (Kunz & Luebbers, 1993). FDTD advantages amongst others include: (1) formulation is easily comprehensible and easy to implement in Matlab, (2) in the time domain analysis a wider range of frequencies can be spanned in just only one simulation, (3) FDTD formulation can work with any dielectric material, environment and computers, (4) the technique fosters an extensive computational efficiency for large problems, (5) FDTD accuracy can be achieved by employing the right cell sizes and (6) FDTD results can help in designing the antenna and provide data on other features such as electrical properties dispersion (Kunz & Luebbers, 1993; Yee, 1966).

The overall goal of this work is to evaluate the use of GPR for non-destructive mapping of seed planting depth after planting. The overall attenuation and the sensitivity of the EM signal through the soil and seed will be analyzed.

Methodology

GPR Operation Principles

A typical GPR systems geometry consists of a transmitter and receiver antennas. To collect data, EM signals are transmitted from a transmitting antenna at high frequency (~10 – 1000MHz) into the ground at a proximal height predetermined by the operator. A pulsing incident signal hits and enters the ground and assuming a lossy dielectric media,

some EM signal pulses are reflected and remaining signals are transmitted into the ground. Reflection occurs when a material with a significant electrical contrast from the host exists within the propagation line. Additionally reflection patterns are depended upon object shape and orientation, relative to EM field polarization vectors and antennae geometry (Neal, 2004). As the EM signal continue propagating, there will be a continual process of reflections and refractions until all the EM signal energy has been dissipated (Sadiku, 2010). Reflected signals are received by the GPR receiver as function of time. From received signal amplitudes, valuable information can be extracted and processed. The operational principle of a GPR system is shown in Figure 1.

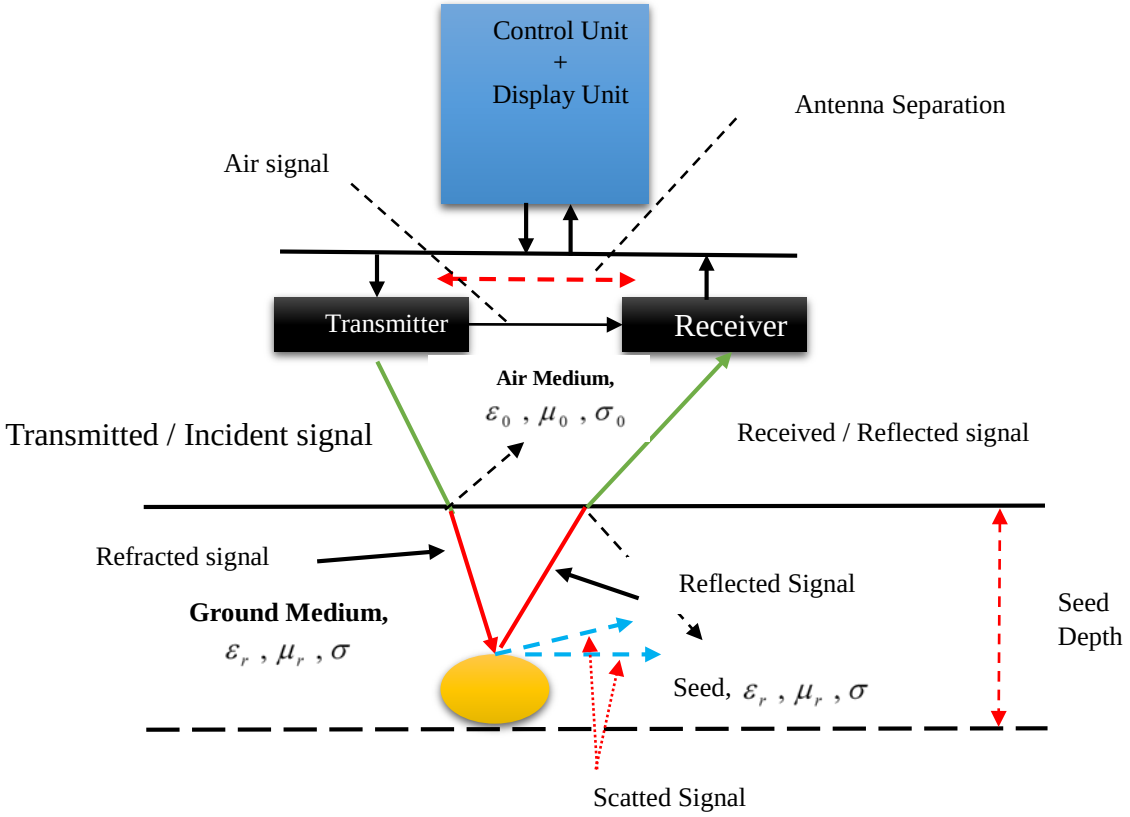

Figure 1. GPR Operational Principles showing antenna separation, air, transmitted, refracted, reflected signals and seed depth (Sato, 2009).

For any GPR system to offer effective performance of the EM signals, the device has to satisfy the following conditions (Daniels, 2004): the EM signal has to be capable of (1) penetrating to desired depths, (2) distinguishing the target from the host i.e. sufficient dielectric contrast and (3) providing an adequate bandwidth for the received EM signal with desired sensor resolution.

Electromagnetics Theory

Electromagnetics involves the study of moving charges on a given space and time. Electromagnetic signals are governed by Maxwell's equations and constitutive laws given hereunder.

Maxwell's Equations

The four major Maxwell's equations are as follows (Jol, 2009; Sadiku, 2010; Wang, 1986):

Faraday's Law:

$$\overline{\nabla} \times \overline{E} = -\frac{\partial \overline{B}}{\partial t} \tag{1}$$

where $\overline{E}$ Electric vector measured in *volts/m*, $\overline{B}$ Magnetic vector field measured in *T*.

Ampere's Law:

$$\overline{\nabla} \times \overline{H} = \overline{J} + \frac{\partial \overline{D}}{\partial t} \tag{2}$$

where $\overline{H}$ Magnetic intensity field measured in *A/m*, $\overline{J}$ Current vector measured in A/m^2, $\overline{D}$ Electric displacement field measured in C/m^2 and

Gauss's Law *(Electric fields)*:

$$\overline{\nabla} \bullet \overline{D} = q \tag{3}$$

where q Electric charge density measured in C/m^3.

In the absence of charge, equation (3) is given as;

Gauss Law without charge:

$$\overline{\nabla} \bullet \overline{D} = 0 \tag{3a}$$

Gauss's Law *(Magnetic fields)*:

$$\overline{\nabla} \bullet \overline{B} = 0 \tag{4}$$

Constitutive Laws

These constitutive parameters form the EM properties of materials. These laws govern the behavior of the EM signals on a medium.

$$\overline{J} = \tilde{\sigma}\overline{E} \tag{5}$$

$$\overline{D} = \tilde{\varepsilon}\overline{E} \tag{6}$$

$$\overline{B} = \tilde{\mu}\overline{H} \tag{7}$$

Dielectric Materials and Properties

Dielectric in its simplest definition refers to a non-conducting material. There are several, well known dielectric materials, these are air, paper, wood, plastics, rubber, salt, cotton, glass, mica, water, soil etc. These dielectric materials all have the distinctive attribute that they consist of polar molecules. These polar molecules are effectively polarized by a changing electric field. During dielectric polarization the charges are shifted and aligned with their opposite charges, leaving a neutral environment between separated charges. As charges align, rate at which the electric field traverse the material slows down (electric field amplitude reduction), the electric field strength reduces and upon completion of charge alignment leads to a zero net electric field across the material. Dielectric materials have dielectric properties. In the study of dielectric materials, the main focus is on electric and magnetic energy storage and dissipation on a material. There are three dielectric properties: (1) dielectric permittivity (measured in Farad/m, F/m), (2) electrical conductivity (measured in Siemens/meter, S/m) and (3) magnetic permeability with a polarization factor measured in inductance per meter (Henry's, H/m) (Annan, 2009; Jol, 2009; Sadiku, 2010). The dielectric properties are defined below.

Permittivity (ε), allows for charge to be stored in a material. The charge stored as a results of the applied electric field is based on the quality of the dielectric material. The larger the permittivity, the higher the electric charge storage and the converse is true (Norimoto, 1976). Permittivity (ε') is given as a product of relative permittivity (ε_r) and permittivity of free space (ε_0): $\varepsilon' = \varepsilon_r\ \varepsilon_0$. When a media is lossy the absolute permittivity (ε) is given as complex function. The imaginary component of the function represents the loss factor (ε'') within a material: $\varepsilon = \varepsilon' - j\varepsilon''$.

Permeability (μ), allows for magnetic field to be supported within a material. Permeable materials are easily magnetized under the influence of the alternating magnetic component of the EM signal pulses. Magnetic permeability can also be expressed as a complex number but in mediums like soil the magnetic losses are often small due to the absence of iron oxide or eddy currents at the interface. Therefore, the imaginary part of the permeability is omitted. However, the property is expressed as product of relative magnetic permeability (μ_r) and permeability of free space (μ_0): $\mu = \mu_r\mu_0$ (Jol, 2009; Neal, 2004; Sadiku, 2010).

Electrical conductivity (σ), a conductivity material effectively conduct the electric component of the EM signal. This property contributes to high EM energy dissipation. Therefore absolute electrical conductivity is expressed as a complex function: $\sigma = \sigma' - j\ \sigma''$ with a loss factor σ'' (imaginary) and actual electrical conductivity σ' (real). These three properties govern EM signals absorption (attenuation), dispersion, phase shift, reflectance on interfacing boundaries and the overall propagation velocity (Orfanidis, 2002). These three electrical properties constitute an effective lossless and lossy media are shown in Table 1.

Propagation of EM signals through Soil

As established, soils are dielectric materials and inherently acts as a lossy media. There natural composition is extremely complex. Their complexity rises from various unconsolidated materials with varying dielectric properties. Their composition includes organic materials, stratigraphy, clay, and water molecules etc. These constituents affect the soil dielectric properties. Signal propagation through soil is governed by the three dielectric properties: permittivity, permeability and electrical conductivity. Using these properties the following propagation relationships can be derived from Maxwell's EM equation: (1) signal reflectance, (2) transmittance, (3) intrinsic impedance, (4) Effective EM signal Attenuation, (5) Effective EM

signal Phase, (6) propagation constant (7) signal velocity. According to (Jol, 2009; Sadiku, 2010), the signal characteristics can be explained using the following equations in Table 1.

Table 1. Governing Equations for Electromagnetic Propagation based on Material Properties.

No.	Relation Name	Equation Governing EM signals Propagation	
8	Effective EM signal Attenuation (Np/m)	$\alpha = \omega\sqrt{\mu\varepsilon}\left(\frac{1}{2}\left[\sqrt{1+\left(\frac{\sigma}{\omega\varepsilon}\right)^2}-1\right]\right)^{1/2}$	This a general formula to compute attenuation α. In a lossless media σ = 0, therefore the attenuation factor becomes; α = 0, no attenuation.
9	Effective EM signal Phase (rad/m)	$\beta = \omega\sqrt{\mu\varepsilon}\left(\frac{1}{2}\left[\sqrt{1+\left(\frac{\sigma}{\omega\varepsilon}\right)^2}+1\right]\right)^{1/2}$	β is the phase shift of the signal or commonly referred to as signal number. Phase shift is temporal on EM signals. It describes the displacement of a signal amplitude from its origin with respect to time. The displacement affect signal velocity. In a lossless media σ = 0, therefore the phase shift is give as; $\beta = \omega\sqrt{\mu\varepsilon}$.
10	Propagation Constant, (γ)	$\gamma = \alpha + j\beta$	A complex number given as function of signal attenuation and signal number/phase shift
11	Intrinsic impedance of the interfacing medium (ohms) (η_i)	$\eta_i = \sqrt{\frac{j\omega\mu_i}{\sigma_i + j\omega\varepsilon_i}}$ $i = 0, 1, 2, 3, 4, 5, \ldots$; Number of mediums	The intrinsic impedance at the interface determines how much portion of the signal is reflected and transmitted. This principle of intrinsic impedance is analogous to Snell's law of refractive index. This relation computes the amplitude and phase of the signal i.e. it's a complex number.
12	Velocity (v) m/s	$v = \frac{1}{\left(\frac{\mu\varepsilon}{2}\left[\sqrt{1+\left(\frac{\sigma}{\omega}\right)^2}+1\right]\right)^{1/2}}$	For a lossless media: $v = \frac{1}{\sqrt{\mu\varepsilon}}$
13	Snell's Law (n)	$n_i \sin(\theta_i) = n_t \sin(\theta_t)$ n_i ; Medium 1 refractive index, n_t ; medium t refractive index, θ_t ; transmission angle	Refractive Index
14	Signal propagation continuity	$\left.\begin{aligned} E_x^{(i)} + E_x^{(r)} &= E_x^{(t)} \\ H_y^{(i)} + H_y^{(r)} &= H_y^{(t)} \end{aligned}\right\}$	E and M continuity at interfacing boundaries
15	EM Reflection, (Γ)	$\Gamma = \frac{\eta_2\cos\theta_i - \eta_1\cos\theta_t}{\eta_2\cos\theta_i + \eta_1\cos\theta_t}$	Reflection Power Factor (Γ): Determines the power of the reflected signal on a media
16	EM Transmission, (τ)	$\tau = \frac{2\eta_2\cos\theta_i}{\eta_2\cos\theta_i + \eta_1\cos\theta_t}$	Transmission Power Factor (τ): Determines the power of the transmitted signal on a media

Signal Reflection and Transmission Coefficients

Portions of the reflected and transmitted EM signals are governed by the equations (15) and (16), in Table 1 (Jol, 2009). These governing equations are expressed as function of the intrinsic impedance, the incident and refractive angles. With Snell's law equation (13) the direction of a reflected and transmitted signal can be determined precisely at each interfacing boundary using the independent refractive index. Further, Snell's law of reflection states that incident angle (θ_i) is equal to reflection angle (θ_r). However, Snell's law given in equation (13) important information about the propagated signal is not

characterized. Therefore, Snell's law alone is not sufficient, since this law does not compute the amplitudes of the reflected and transmitted Electric (E) and Magnetic (M) fields. Prediction of the E and M field amplitudes for a propagating signal are approximated using Fresnel's formulae, coupled with each medium's boundary conditions. As a rule of thumb, to ensure continuity of the propagating signal, the E and M fields must be continuous at the interface boundary. This means the E incident and reflected signals must equal the E transmitted (total) signal, as shown in equation (14). The same principles applies to M fields. For example, suppose a signal is propagated along z-direction and E and M fields are along x and y directions respectively, then the principles in equation (14) have to be satisfied (Kunz & Luebbers, 1993; Born & Wolf, 1999; Jol, 2009).

Manipulation of the incident, reflected and transmitted fields in equation (14) into respective components equations (15) and (16) are obtained. These equations satisfies signal propagation reflection and transmission as well as E and M continuity at interfacing boundaries (Born & Wolf, 1999; Orfanidis, 2002). Equations (15) and (16) represents reflection and transmission coefficients, respectively. The reflectance and transmittance coefficients are used to determine the amount of reflected and transmitted energy.

FDTD Formulation and Engine

The Gaussian equations in (3a) and (4) portraying a zero divergence consequently forces E and M fields to travel perpendicular to direction of propagation. Signals generated through this phenomenon are termed planar signals. The antecedent of the Maxwell's curl equations exist when there is an oscillatory motion of the E and M fields with respect to space and time along a specified propagation line. In real time signals updates and oscillates simultaneously for specified period of time. But, FDTD model fields update sequentially by calling the Maxwell's curl equations (1) and (2) coupled with constitutive equations (3) – (5).

In FDTD models the current, $\overline{J}$ can be ignored (or $\overline{J} = 0$) when modeling a signal in a dielectric media in free space (i.e. a linear, isotropic and nondispersive material) because there are no metals and currents, but in cases where losses need to be included in the model, this term needs to be part of the FDTD simulation models. Substituting constitutive equations into Maxwell curl equations, following equations are obtained:

$$\overline{\nabla} \times \overline{E} = -\mu \frac{\partial \overline{H}}{\partial t} \tag{17}$$

$$\overline{\nabla} \times \overline{H} = \sigma \overline{E} + \varepsilon \frac{\partial \overline{E}}{\partial t} \tag{18}$$

These equations forms the basic model of the FDTD. The basic FDTD engine employs the leapfrog principle (Yee, 1966) which enables the models to update the fields sequentially. In equation (17) the curl of the electric field is calculated and divided by the permeability which gives the magnitude of the changing $\overline{H}$ field at the center of the curl. Basically the $\overline{H}$ field is updated from the curl of the $\overline{E}$ field. In exact same manner, in equation (18) $\overline{E}$ field is updated from the curl of $\overline{H}$. Ultimately the algorithm bounces back and forth updating $\overline{E}$ and $\overline{H}$ for a finite period of time. This is a typical setup for the FDTD engine.

Finite Difference Approximation

FDTD models use the central finite differences or central differences method to compute the EM fields. This method to be precise, estimates the midpoint between two consecutive points on the grid (i.e. points f_1 and f_2), to predict the gradient of a function. The gradient is the rise over spatial change (i.e. Δx). Therefore, all derivatives of the Maxwell's curl equations in our FDTD models are represented by central finite differences keeping in mind that, each term must exist at the same point in time and space. Also by placing central differences for derivatives improves the stability of FDTD models. The Central Difference Method (Schneider, 2010; Warnick, 2011)

$$\frac{f(x+\Delta x) - f(x)}{\Delta x} + \frac{f(x+\Delta x) + f(x)}{2} = 0 \tag{19}$$

This is a very important rule on estimating EM fields using the FDTD technique. Using the finite differencing rule, the time derivatives of Maxwell curl equations (17) and (18) can be approximated as shown in (20) and (21). This framework is basically the core of the finite differencing method. The $\overline{E}$ and $\overline{H}$ are staggered in time. By staggering fields allows for $\overline{E}$ and $\overline{H}$ to exist half time step apart: $\overline{\mathbf{E}}(t)$ exist at integer time, t whilst $\overline{\mathbf{H}}(t \pm \Delta t/2)$ exist at past and future half time step, henceforth,

$$\overline{\nabla} \times \overline{\mathbf{E}}(t) = -\mu \frac{\overline{\mathbf{H}}(t + \Delta t/2) - \overline{\mathbf{H}}(t - \Delta t/2)}{\Delta t} \tag{20}$$

$$\overline{\nabla} \times \overline{\mathbf{H}}(t + \Delta t/2) = \sigma \overline{\mathbf{E}}(t + \Delta t/2) + \varepsilon \frac{\overline{\mathbf{E}}(t + \Delta t) - \overline{\mathbf{E}}(t)}{\Delta t} \quad \Leftrightarrow$$

$$\overline{\nabla} \times \overline{\mathbf{H}}(t + \Delta t/2) = \sigma \frac{\overline{\mathbf{E}}(t + \Delta t) + \overline{\mathbf{E}}(t)}{2} + \varepsilon \frac{\overline{\mathbf{E}}(t + \Delta t) - \overline{\mathbf{E}}(t)}{\Delta t} \tag{21}$$

The vector equations (20) and (21) are stable and presents valid central finite differencing in approximating $\overline{E}$ and $\overline{H}$ fields. From these models updating equations can be resolved, by manipulation of $\overline{E}$ and $\overline{H}$ term. The terms $\overline{\mathbf{H}}(t \pm \Delta t/2)$ are defined for the magnetic field to exist at those half time steps.

Predicting Equations

From vector equations (20) and (21), the field equations can be derived. The derivation is based on resolving models for each future half time step and time step of the magnetic and electric fields, respectively i.e. $\overline{\mathbf{H}}(t + \Delta t/2)$ and $\overline{\mathbf{E}}(t + \Delta t)$ (Schneider, 2010):

$$\overline{\mathbf{H}}(t + \Delta t/2) = \overline{\mathbf{H}}(t - \Delta t/2) - \frac{\Delta t}{\mu} \left| \overline{\nabla} \times \overline{\mathbf{E}}(t) \right| \tag{22}$$

$$\overline{\mathbf{E}}(t + \Delta t) = \left(\frac{2\Delta t}{\sigma \Delta t + 2\varepsilon} \right) \left| \overline{\nabla} \times \overline{\mathbf{H}}(t + \Delta t/2) \right| - \left(\frac{\sigma \Delta t - 2\varepsilon}{\sigma \Delta t + 2\varepsilon} \right) \overline{\mathbf{E}}(t) \tag{23}$$

Anatomy of the Predicting Equations

Equations (22) and (23) are the fundamental equations used to predict the electric fields. In equation (22) the future magnetic field at half time step $\overline{\mathbf{H}}(t + \Delta t/2)$, is updated by using the past magnetic field at previous half time step $\overline{\mathbf{H}}(t - \Delta t/2)$ and subtracting the correction factor of the curl equation $\left| \overline{\nabla} \times \overline{\mathbf{E}}(t) \right|$ at time, *t*, multiplied by $\Delta t/\mu$. The term $\Delta t/\mu$, can be a constant factor or time changing factor as signal propagates through a dielectric media.

In equation (23) the future electric field at time step $\overline{\mathbf{E}}(t + \Delta t)$, is updated by evaluating the difference between the future curl equation $\left| \overline{\nabla} \times \overline{\mathbf{H}}(t + \Delta t/2) \right|$ at the intermediate half time step multiplied by $\left(2\Delta t/\sigma \Delta t + 2\varepsilon\right)$ and the past electric field $\overline{\mathbf{E}}(t)$ at previous time step *t*, multiplied by $\left(\sigma \Delta t - 2\varepsilon/\sigma \Delta t + 2\varepsilon\right)$. In addition, the two coefficients of the equations can be defined as constants or time varying. In a lossless, isotropic and nondispersive media, all coefficients are constants whilst in lossy, anisotropic, and dispersive media coefficients are spatially varying.

Time Step, Cell Size, Sampling Rate and Absorbing Boundary Conditions

Selecting time step, cell size, sampling rate and boundary conditions are the most important aspect of the FDTD formulation. *Cell sizes* enhances FDTD accuracy at high frequencies. Material properties have potential to affect cell sizes used in the simulation. The cell step sizes (i.e. Δx) need to be smaller than the smallest wavelength to attain accuracy. To estimate the cell size sampling is used. *Sampling rate* is an important component when simulating FDTD. The sampling rate used on FDTD models must follow the Nyquist sampling rate principle, which states that, 'to be able to reconstruct a signal and avoid aliases, a signal has to be sampled at least twice the frequency.' Commonly used sampling rates in signal processing are usually greater than standard Nyquist sampling rate specified i.e. $\lambda \geq 2f$ (λ *and* f wavelength and frequency). When sampling, the FDTD uses temporal and spatial resolution i.e. $\lambda \geq 2\Delta x$ (λ wavelength). In FDTD modeling, the rate at which the $\overline{E}$ and $\overline{H}$ are sampled ranges from $10\Delta x \quad to \quad 20\Delta x$, for low contrasting dielectrics Upon determining the cell size, a time step may be computed using a Courant Stability Condition (CSC), following the rule of thumb that, the propagated EM signal velocity cannot surpass the speed of light. The CSC is a normalizing factor, which normalizes the fields. CSC is normally equal or less than one. The CSC for one dimensional FDTD is expressed as: $\Delta t \leq \Delta x/C$, where *C* is the speed light. Time steps are required to show progression of the signal in a problem space domain. Time steps are not in any way linked to FDTD models accuracy. However, larger time steps are undesirable as they can lead to instability (Kunz & Luebbers, 1993; Ketata et al., 2010). Absorbing boundary conditions (ABC) need to be

implemented on model to effectively truncate the mesh of the tangential fields and prevent reflection of the signal at the end of the computational space, back into the computational space (Mur, 1981, 1998; Schneider, 2010).

1D FDTD Formulation and Implementation in Matlab

Updating equations (22) and (23) are used to build 1D FDTD model. 1D FDTD model will propagate electric and magnetic field signals through a defined problem space domain. Two lossy mediums are imposed on the signal path. First, field domains are defined: hereunder, signal propagation direction for the 1D FDTD is considered to be along z-direction and the electric and magnetic fields to be along y and x-directions, respectively. Therefore, Maxwell's curl equations (17) and (18) are presented with spatial domain script;

$$\overline{\nabla} \times \overline{\mathbf{E}_y} = -\mu \frac{\partial \overline{\mathbf{H}_x}}{\partial t} \qquad \overline{\nabla} \times \overline{\mathbf{H}_x} = \sigma \overline{\mathbf{E}_y} + \varepsilon \frac{\partial \overline{\mathbf{E}_y}}{\partial t}$$

Transforming these spatial defined equations to first order updating equations, the method used by (Schneider, 2010) is followed;

$$\overline{\nabla} \times \overline{\mathbf{E}_y} = \begin{vmatrix} a_x & a_y & a_z \\ 0 & 0 & \frac{\partial}{\partial z} \\ 0 & \overline{\mathbf{E}_y} & 0 \end{vmatrix} = -a_x \frac{\partial \overline{\mathbf{E}_y}}{\partial t} = -\mu \frac{\partial \overline{\mathbf{H}_x}}{\partial t} \quad \Rightarrow \quad \frac{\partial \overline{\mathbf{E}_y}}{\partial t} = \mu \frac{\partial \overline{\mathbf{H}_x}}{\partial t} \tag{24}$$

$$\overline{\nabla} \times \overline{\mathbf{H}_x} = \begin{vmatrix} a_x & a_y & a_z \\ 0 & 0 & \frac{\partial}{\partial z} \\ \overline{\mathbf{H}_x} & 0 & 0 \end{vmatrix} = a_y \frac{\partial \overline{\mathbf{H}_x}}{\partial z} = \sigma \overline{\mathbf{E}_y} + \varepsilon \frac{\partial \overline{\mathbf{E}_y}}{\partial t} \quad \Rightarrow \frac{\partial \overline{\mathbf{H}_x}}{\partial z} = \sigma \overline{\mathbf{E}_y} + \varepsilon \frac{\partial \overline{\mathbf{E}_y}}{\partial t} \tag{25}$$

Using the fields leapfrog principle, the two scalar equation are transformed to predict future values. The transformed equations are used to build a functional Matlab program for simulation and material properties of a lossy and dispersive media are defined in Matlab code.

$$\overline{H}_x^{\,n}\Big|_{t+\frac{\Delta t}{2}} = \overline{H}_x^{\,n}\Big|_{t-\frac{\Delta t}{2}} + \frac{c\Delta t}{\mu \Delta z}\left(\overline{E}_y^{\,n+1}\Big|_t - \overline{E}_y^{\,n}\Big|_t\right)$$

$$\overline{E}_y^{\,n}\Big|_{t+\Delta t} = \left(\frac{2c\Delta t}{(\sigma\Delta t + 2\varepsilon)\Delta z}\right)\left(\overline{H}_x^{\,n}\Big|_{t+\frac{\Delta t}{2}} - \overline{H}_x^{\,n-1}\Big|_{t+\frac{\Delta t}{2}}\right) + \left(\frac{\sigma\Delta t - 2\varepsilon}{\sigma\Delta t + 2\varepsilon}\right)\overline{E}_y^{\,n}\Big|_t$$

Secondly, boundary conditions are defined. A grid length of N is required for the 1D FDTD simulation. Since grid length is equal to *N*, then component, $\overline{E}_y^{\,n+1}\Big|_t$ and $\overline{H}_x^{\,n-1}\Big|_{t+\Delta t/2}$ do not exist. These two terms are set to zero and the Dirichlet boundary are set at $n = 1 : N-1$ for magnetic field and $n = 2 : N$ for electric field

$$for \quad n = N \Rightarrow \overline{H}_x^{\,n}\Big|_{t+\frac{\Delta t}{2}} = \overline{H}_x^{\,n}\Big|_{t-\frac{\Delta t}{2}} + \frac{c\Delta t}{\mu \Delta z}\left(0 - \overline{E}_y^{\,n}\Big|_t\right)$$

And,

$$for \quad n = 1 \quad \Rightarrow \overline{E}_y^{\,n}\Big|_{t+\Delta t} = \left(\frac{2c\Delta t}{(\sigma\Delta t + 2\varepsilon)\Delta z}\right)\left(\overline{H}_x^{\,n}\Big|_{t+\frac{\Delta t}{2}} - 0\right) + \left(\frac{\sigma\Delta t - 2\varepsilon}{\sigma\Delta t + 2\varepsilon}\right)\overline{E}_y^{\,n}\Big|_t$$

Signal Source

In this study a simple Gaussian pulse is used to evaluate the effects caused by the relative dielectric permittivity, permeability and electrical conductivity of the soil and seed on the overall performance of the propagating signal. Figure 2

represents a Gaussian source.

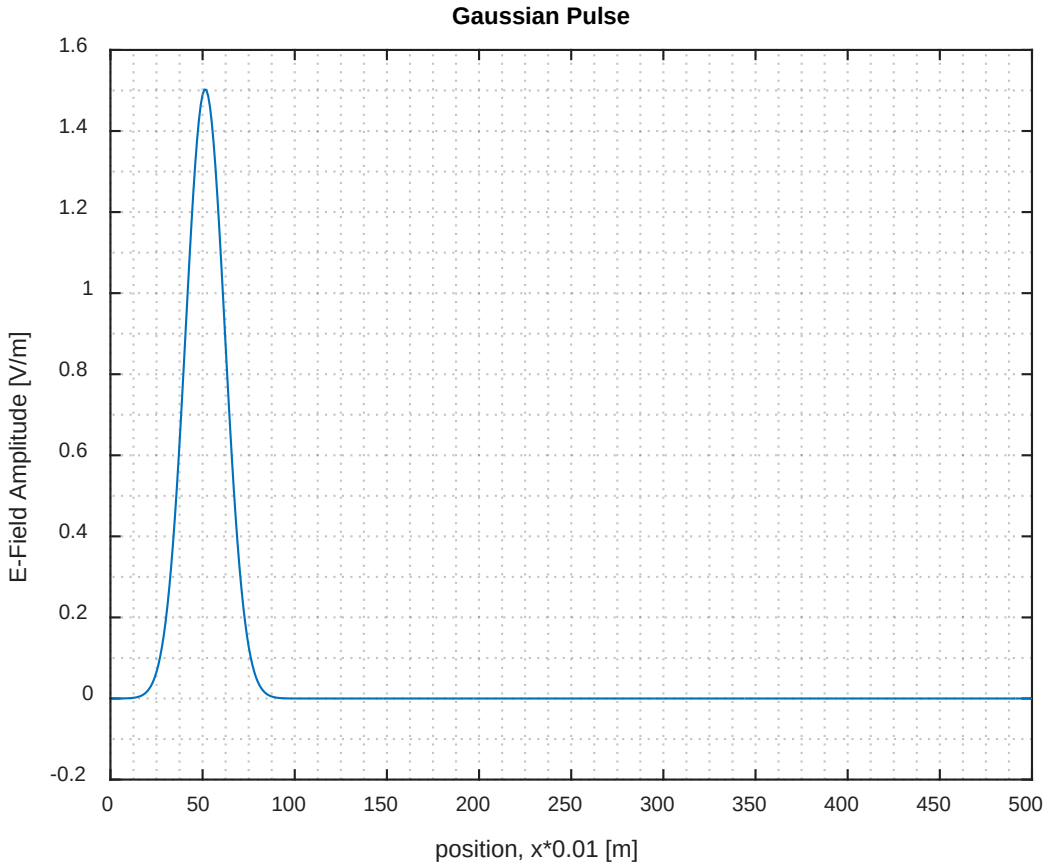

Figure 2. This a simple Gaussian Pulse used in Analysis the behavior of the EM signals on a dielectric medium. The pulse operate at frequency of 1 GHz with an Initial Electric Field Strength of 1.5 Volts/meter

The equation used to generate the Gaussian pulse in figure 2 is given as

$$Esrc(t) = A\exp^{-\frac{(t-t_0)}{\tau}} \tag{26}$$

where, *Esrc* – Gaussian source at time ***t***., *A* – Signal amplitude and τ – width time of the Gaussian pulse

Planted Seed Model

The transmitting antenna is located two meters from the soil and the planted seed is placed fifty centimeter in the soil. In between the transmitting antenna and the soil the signals travel through an air layer. Air losses in the study are neglected (zero). The model in Figure 3 is composed of two relevant layers, soil layer and the seed layer as characterized by their respective electrical properties. ABC are implemented as shown in Figure 3.

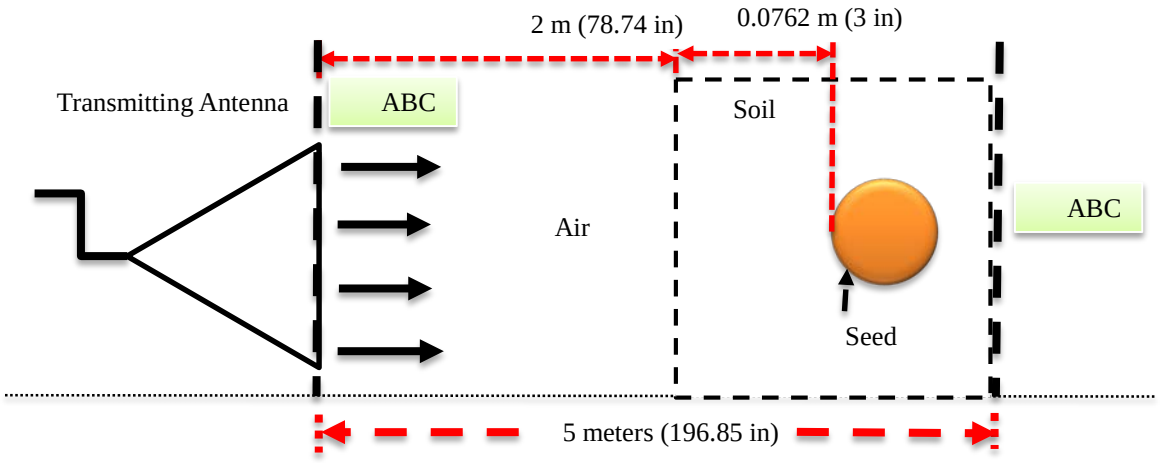

Figure 3. A simple model of a Planted Seed on Soil.

Table 2. Material Properties: Volumetric Moisture Content, Relative Dielectric Permittivity and Electrical Conductivity used in the Matlab simulation (Daniels, 2004; Attia al Hagrey, 2007; Jol, 2009).

Material	Volumetric Moisture Content (%)		Soil Electrical Properties	
			Permittivity, ε_r	Conductivity, σ (mS/m)
Air	---		1	---
Sandy	Dry	5.50	4	0.10
		14.76	8	3.00
		27.58	15	10.00
	Wet	44.41	30	100.00
Loamy /Silt	Dry	5.53	4	0.10
		10.33	6	1.00
		18.83	10	10.00
	Wet	34.54	20	100.00
Clay	Dry	5.53	4	0.10
		10.33	6	100.00
		18.83	10	100.00
	Wet	27.58	15	1000.00
Corn seed	---		2.67	---

Normally the volumetric moisture content of field soils during growing season range from 15 – 40 percent (Weiler, Steenhuis, Boll, & Kung, 1998). The volumetric moisture content is an important factor for the simulation. The empirical permittivity values in Table 2, are useful in predicting the volumetric moisture content (VMC) of the soil. Based on the permittivity (Topp, Davis, & Annan, 1980) established a model to predict VMC of the soil with accuracy of $\pm 2\%$. In the psychrometric chart the VMC has to between the residual water content and saturation point to successfully supply water to seeds (Hillel, 2003; Tuller & Or, 2004). The residual water content is the bound water held between soil particles at high potential pressure and this water cannot be used by the seeds. This is referred to as the wilting point and osmotic water suction is impossible. Saturation ranges from 0 to 1, and beyond saturation maximum point soils are very wet and this can hinder seed germination due to suffocation and excess oxygen. The residual water content and saturation points for each soil type are: sandy 0.054 and 0.37, loam-silt 0.061 and 0.43 and clay 0.102 and 0.51, respectively. Desired ranges for seed germination are within the residual water content and saturation point and each soil type has different VMC characteristics. The characteristics are highly influenced by the porosity and pore size. Additional information on soil water characteristics is presented by the following authors (Isselstein et al, 2002; Hillel, 2003; Tuller & Or, 2004). This studies simulation models are based on the VMC values conducive for seed germination.

Results and Discussions

Isolating electrical properties

The isolation of properties is only done using one layer to help analyze the effect of a single property with the exception of permeability which is assumed to be 1 for all simulation cases. A frequency of 1 gigabytes was used for the simulations.

Effect of Dielectric permittivity

The response signals in the graphs are extracted at three different time steps to show the progression of the signal.

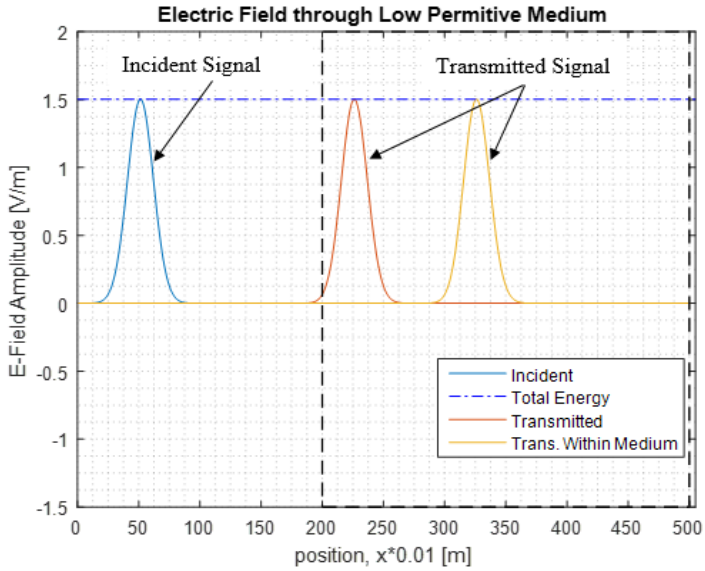

(a) Air Medium with Permittivity of 1

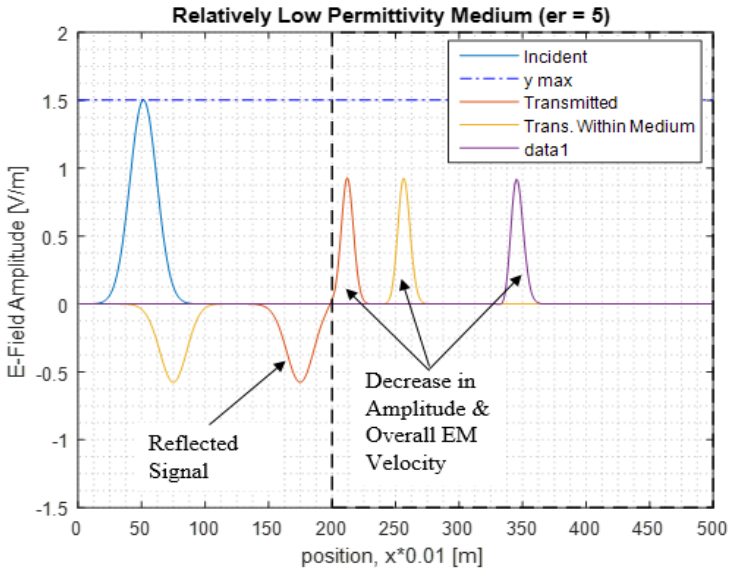

(b) Medium with Permittivity of 5

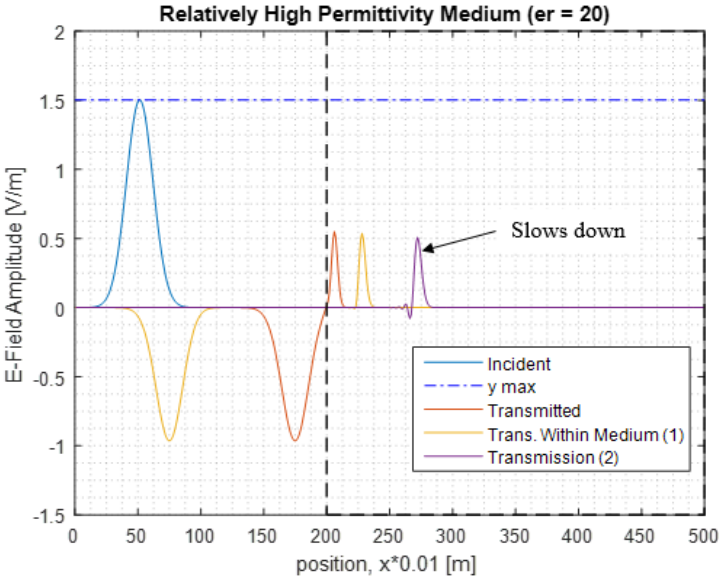

(c) Medium with Permittivity of 20

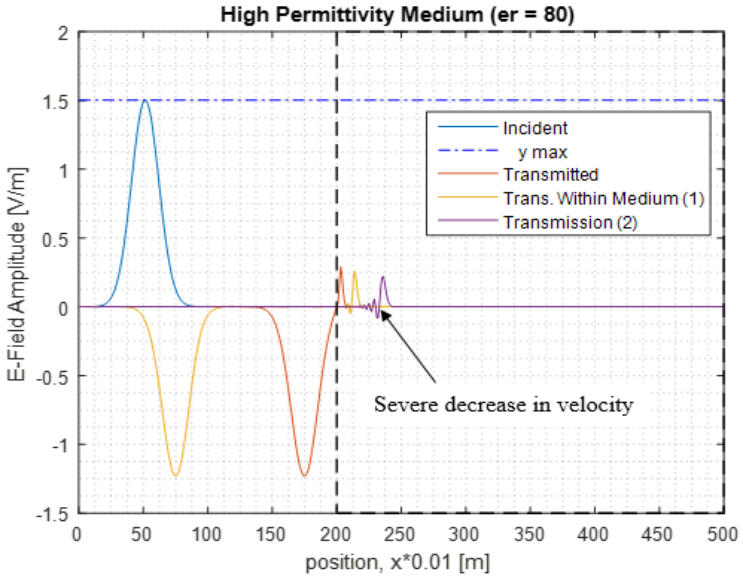

(d) Medium with Permittivity of 80

Figure 4. Isolation of Dielectric Permittivity to evaluate the performance of EM Signal based on different Permittivity values, corresponding to low permittivity medium, air εr = 1 (a, top left) Medium permittivity medium εr = 5 (b, top right), relatively high permittivity medium ε_r = 20 (c, bottom left), high permittivity medium ε_r = 80 (d, bottom right).

Figure 4a shows the Propagation of EM signal through free space (Air) at a constant frequency of one gigahertz (1 GHz), the magnitude of the incident and transmitted signal amplitude are equal. In this case, there is no signal reflection and attenuation through air, and 100 percent of the signal is transmitted. At the boundary the EM signal is completely absorbed. A change in the peak represents the presences of a unique medium along the EM signal path. The magnitude of peak change is proportional to the magnitude of the property effecting the change i.e. permittivity. In figures 4a – 4d represents different

levels of permittivity (low to high) and the influence of the permittivity on the EM signal is distinct with each level. The smaller the permittivity, the smaller the reflected signal and a considerable reduction of the signal amplitude through the medium. Conversely, high permittivity leads to increased reflections, Figures 4c – 4d. As the signal traverses a small reduction on the signal amplitude is noticeable. This phenomena is due to the intrinsic impedance of the material. Intrinsic impedance affects the wavelength and velocity of the signal, hence the signal energy gets stored within a medium as it cannot travel any fast due to material resistance.

Effect of Electrical conductivity

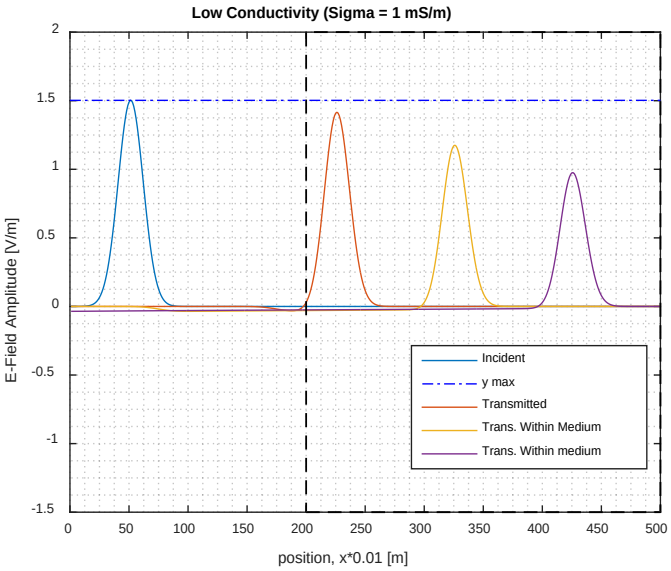

(a) A low conductive medium – 1 mS/m

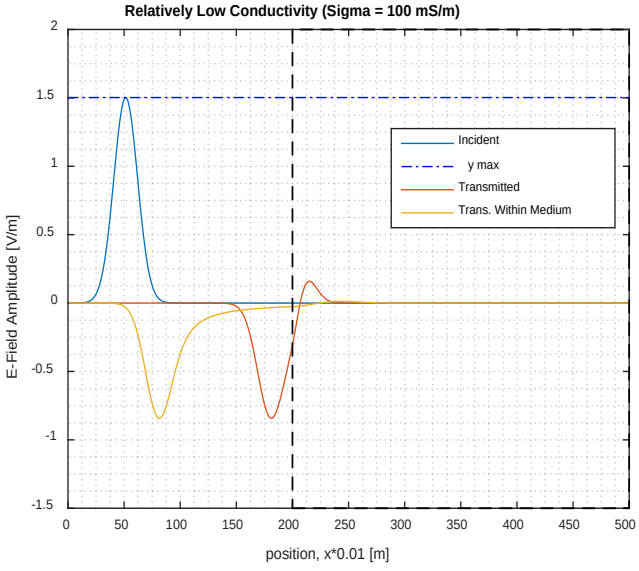

(b) Medium with Electrical conductivity of 100 mS/m

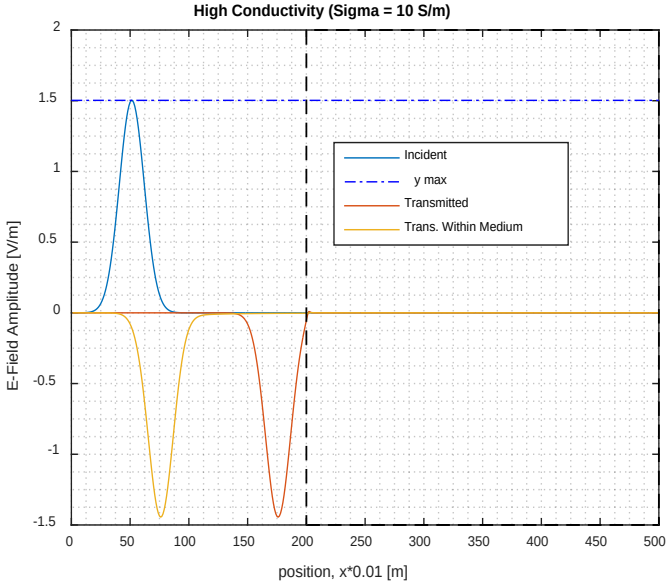

(c) Medium with Electrical conductivity of 10 S/m

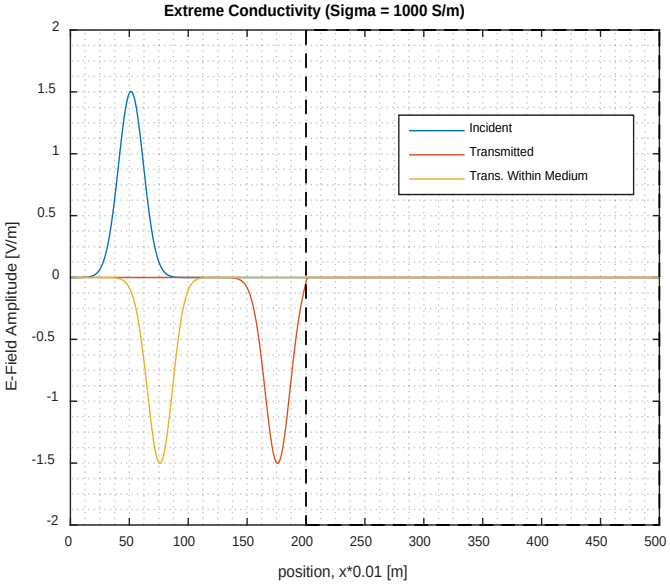

(d) Medium with Electrical conductivity of 1000 S/m

Figure 5. Isolation of Electrical Conductivity to evaluate the performance of EM Signal based on different Electrical Conductivity values, corresponding to low Electrical Conductivity medium, σ = 1 mS/m (a, top left), relatively low Electrical Conductivity medium σ = 100 mS/m (b, top right), relatively high Electrical Conductivity medium σ = 10 S/m (c, bottom left), high Electrical Conductivity medium σ = 1000 S/m (d, bottom right).

The EM signal is highly sensentive to a highly conducting materials as clearly shown in Figures 5a through 5d. A gradual increase in the electrical conductivity values, leads to high attenuation of the EM signal . The signal is highly sensitivity to electrical conductivity of the medium. Smaller electrical conductivity values i.e. 0.001 Sm^{-1} leads to a tolerable signal attenuation i.e. the signal decay across the material is less rapid. However, with high conductive materials the signal barely

or fails to penetrate the material, hence rendering mapping the internals of the material impossible. Based on the isolation of properties a summarry can be drawn in this study that, in highly permittive and conductive soils GPR-EM signals to map the seed planting depth, may not be possible.

Planted Seed model

The interaction of the EM signal with different soil types and the seed which has constant dielectric property is analyzed i.e. amount of signal reflected by the soil and seed, transmitted and the overall attenuation of the signal as it interacts with soil and the seeds. Seed dielectric properties used in the simulation were $\varepsilon_r = 2.67$, $\mu_r = 1.00$ and $\sigma = 0.00$ and frequency of 1 GHz remain unchanged for the entire simulation.

Sandy Soil

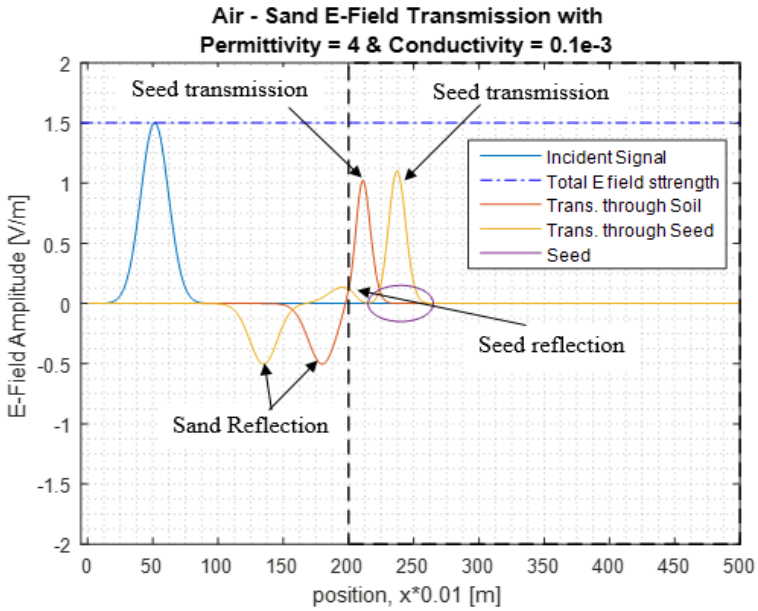

(a) Gaussian Pulse propagated through Air-Sand and seed, with Sand soil permittivity $\varepsilon_r = 4$, $\sigma = 0.1$ mS/m

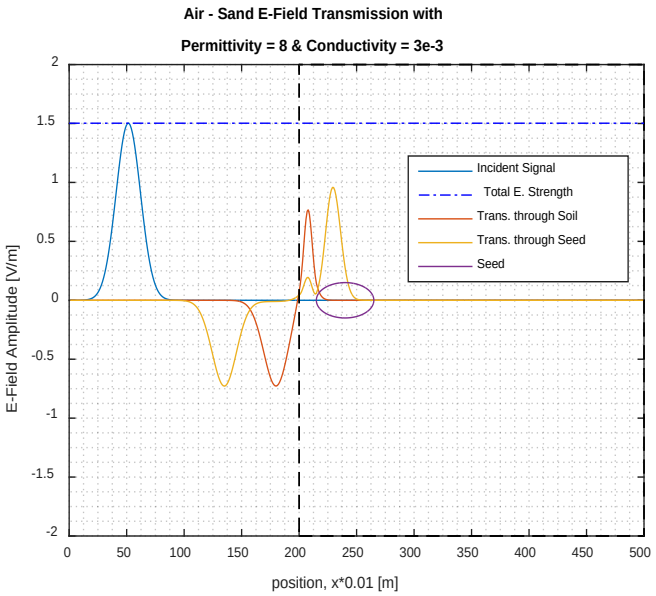

(b) Gaussian Pulse propagated through Air-Sand and seed, with Sand soil permittivity $\varepsilon_r = 8$, $\sigma = 3$ mS/m

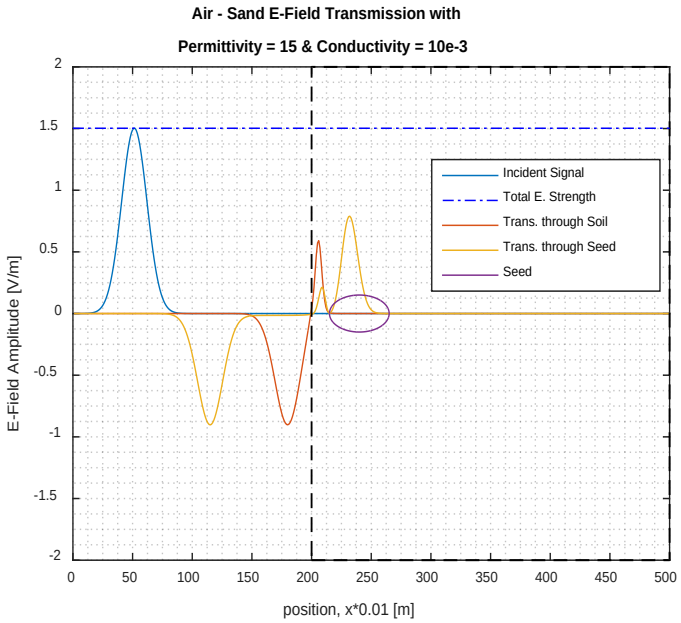

(c) Gaussian Pulse propagated through Air-Sand and seed, with Sand soil permittivity $\varepsilon_r = 15$, $\sigma = 10$ mS/m

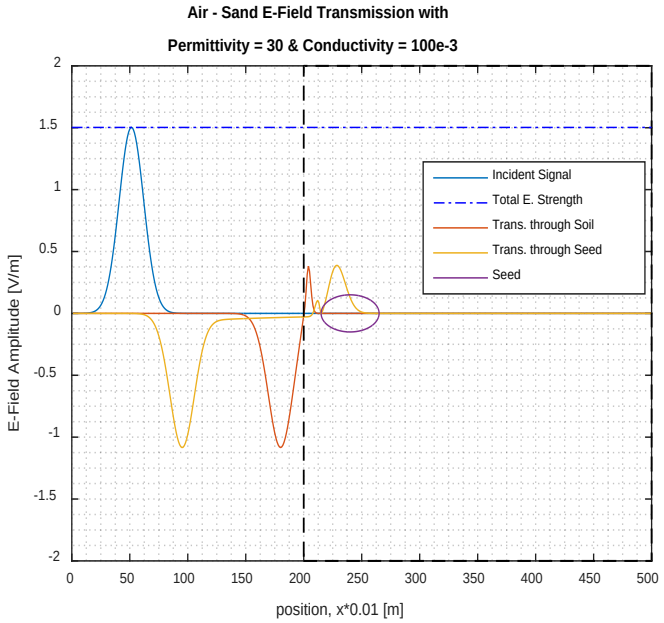

(d) Gaussian Pulse propagated through Air-Sand and seed, with Sand soil permittivity $\varepsilon_r = 30$, $\sigma = 100$ mS/m

Figure 6. Evaluation of EM Signal through Sandy soil and the Seed. The performance of the EM Signal is based on different dielectric permittivity and Electrical Conductivity values for the sand as well as seed electrical properties. Dielectric permittivity and Electrical Conductivity values increase from low permittivity and conductivity $\varepsilon_r = 4$, $\sigma = 0.1$ mS/m (a, top left) to high permittivity and conductivity $\varepsilon_r =$

30, σ = 100 mS/m (d, bottom right).

Clay Soil

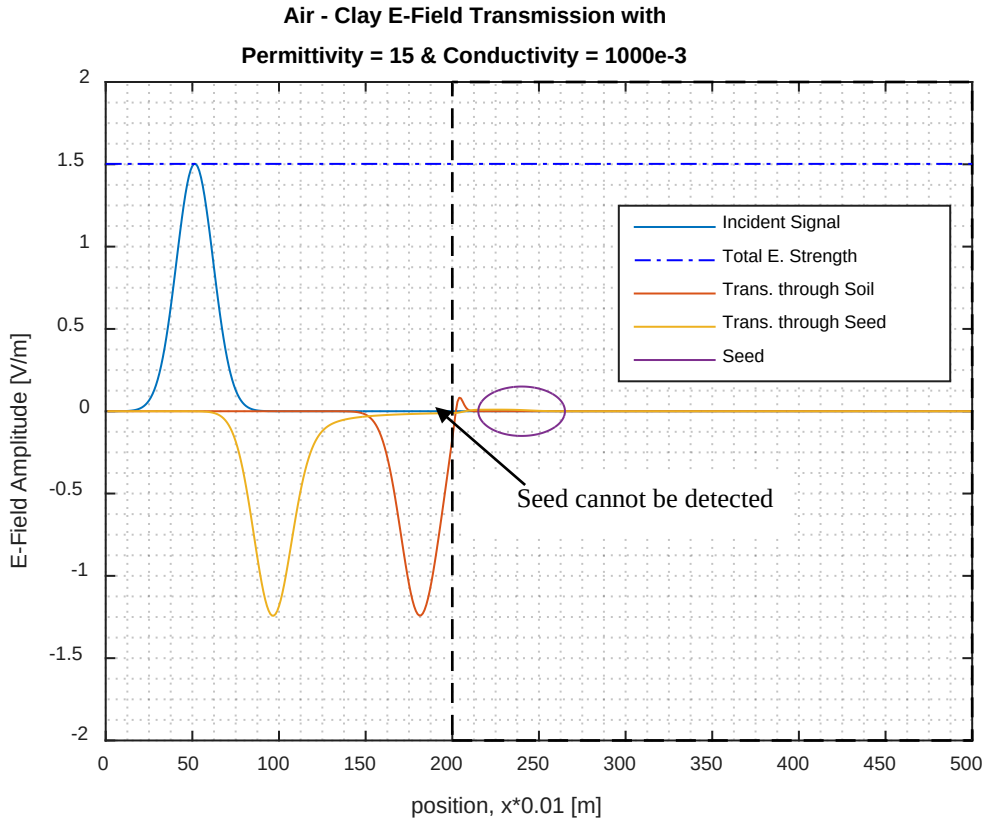

Figure 7. Propagation of EM (E-field) signal through a Lossy Clay Soil.

In Figures 6a through 6d and 7, the permittivity and conductivity are infused to evaluate responses through air and different soil types. The effects of these properties are studied above and this section (planted seed model) investigates feasibility of using GPR to map seed planting depth in different soil types classified by their electrical properties and volumetric moisture content. Along the position axis the soil boundary starts at 200 through 500 centimeters (cm) whilst the seed is placed at 207.62 cm (3 inches) from top soil, for all soil types. All soil types are considered homogenous and seed property is constant throughout simulation. The magnitude of the soil reflection amplitude across each plot is clearly seen as the inverted signal at boundary point and this reflection can be captured by the GPR receiver.

On the other hand, seed reflection amplitude is clearly visible for the first 4 simulation results, Figures 6a to 6d. Though visible the reflected amplitudes are significantly smaller. This implies that GPR can be used to map the seed planting depth in homogenous soils. However, presents challenges in heterogeneous soils where electrical properties are varying with depth. Several scenarios may occur, such as reflected signal scattering within the soil hence failing to surface to be captured by the GPR receiver. Figure 6d and 7 present's impenetrable soils. The EM signals in these figures attenuates at a fast rate. In figure 6d, only a small transmitted signal reaches the seed boundary and the reflection from the seed is barely noticeably. In figure 7, the signal barely enters clay soil surface but fails to reach seed wall. In this phenomenon, mapping the subsurface is impossible, and hence the seed goes undetected. In such cases the GPR cannot be used as viable tool to map seed planting depth. The overall attenuation of the signal across air and each soil type are presented in Table 3.

Table 3. Sensitivity results based on Dielectric Properties of the Soil and Planted Seed.

Media	Volumetric Moisture Content (%)	Dielectric Permittivity	Attenuation (dB/m)
Air	0.00	1.00	0.00
Sand	5.50	4.00	-2.18
	14.76	8.00	-14.90
	27.58	15.00	-288.18
	44.41	30.00	-777.29

Air	0.00	1.00	0.00
	5.53	4.00	-2.18
Loam - Silt	10.33	6.00	-4.10
	18.83	10.00	-264.49
	34.54	20.00	-704.53
Air	0.00	0.00	0.00
	5.53	4.00	-2.18
Clay	10.33	6.00	-499.40
	18.83	10.00	-578.49
	27.58	15.00	-845.64

Overall Attenuation

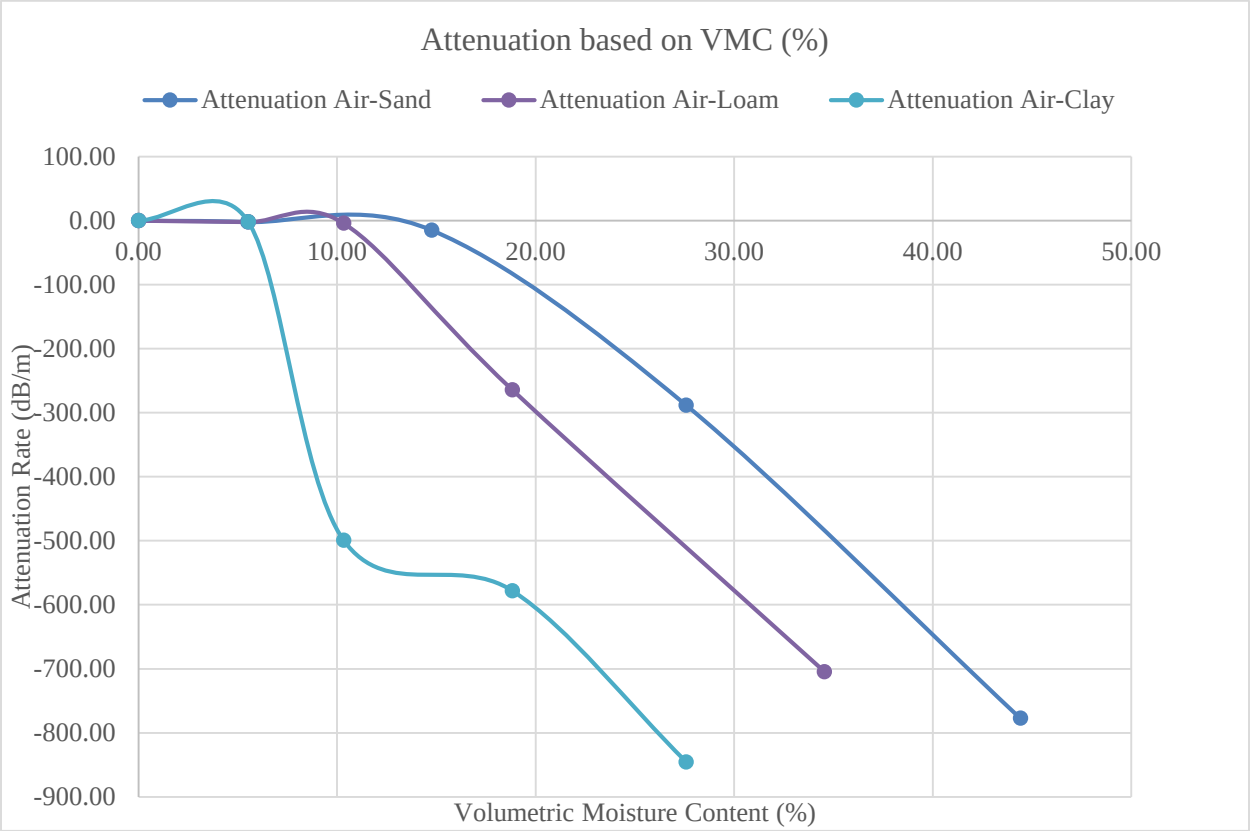

Figure 8. EM pulse signal Attenuation per Soil Type.

Figure 8 summarizes the data in Table 3 and the linear behavior of the line shows attenuation of the signal of each soil type at different volumetric moisture contents. Some of the soil properties in Table 2 are not presented in the simulation results because most of them are encapsulated within sand electrical properties. Wet sand and clay leads to a great deal of the EM signal to be attenuated making mapping the seed practically impossible. Slopes in Figure 8 shows each soil type attenuation rate. The information is critical in selecting GPR system to use on mapping targets of interest.

Conclusion

In the isolation process it is clear that, the penetration of the EM signal is governed by the permittivity and electrical conductivity of the ground soil. Therefore, it is apparent from these two medium (soil) properties that prior to conducting experiment, these properties need to be understood to succinctly map seed planting depth. High values of either, are detrimental to the EM signal propagation through soils. In the simulation results the following observations were made,

(1) High permittivity renders a material to act as a buffer i.e. the signal spends long time within the medium, due the medium impedance, hence a reduction in signal velocity. Conversely, in a low permittivity space the EM signal amplitude and velocity increases. Air has a hundred percent transmittance of the EM signal hence zero reflectance and
(2) The EM signal is highly sensitive to electrical conductivity. A highly conductivity material prevents the signal to penetrate the medium. All signal energy gets reflected and for low conducting materials, a portion of the signal penetrates but slowly attenuates to zero.

Soil and the seed are two homogenous lossy layers. The homogeneity of these layers are based on the depth and time invariant dielectric constants. For each soil type, values are altered to represent different volumetric moisture content of the soil. It is evident that as volumetric moisture content increases the permittivity and electrical conductivity of the soil increases as well, leading to significant EM signal attenuation through the soils. Attenuation rates of the EM signal through each soil type are shown. At the highest volumetric moisture content the attenuation is severe compared to dryer soils. This gives an idea of which conditions are suitable to operate the GPR system. For instance, wet sandy and clay soils need to be avoided, since the attenuation is high and significant energy is lost in the soil medium. For low volumetric moisture content soils, the seed can be detected. However, the reflection signal from the seeds has a small signal amplitude. In this case the signal is weak and it may fail to surface to be captured by the GPR receiver. The weak reflected signal is due to the lack of sufficient dielectric contrast between soils and the seed. The dielectric contrast between the soil and seed is minimal, at moderate volumetric moisture content, and typical soils have dielectric permittivity range of 4 to 6, compared to seeds which have a dielectric permittivity less than 3 (naturally dry sown seeds have a low dielectric permittivity). Though the GPR can be used as a viable tool to map the seed planting depth, the latter presents challenges to map the seed planting depth on different soils with varying volumetric moisture content. Successful and precisely mapping the seed planting depth, may require enhancements of the seed electrical properties to enable the GPR to definitively map the seed planting depth on a closed trench. For instance, increasing the electrical conductivity of the seed i.e. coat the seed with conductive layer capable of melting away after minutes of planting and the conductive coat has to be harmless to the physical and chemical properties of the seed. This procedure ensures that there is sufficient dielectric contrast between the soil and the seed. Electrical conductivity has shown to be effective in blocking the EM signal from penetrating the medium, hence a strong reflection from the boundary of the material. The manipulation of this property, may allow GPR to successful and accurately map the seed planting depth on a closed trench.

References

Allred, B., Daniels, J., Fausey, N., Chen, C., Peters Jr, L., & Youn, H. (2005). Important considerations for locating buried agricultural drainage pipe using ground penetrating radar. *Applied engineering in agriculture, 21*(1), 71-87.

Allred, B., Fausey, N., Peters Jr, L., Chen, C., Daniels, J., & Youn, H. (2004). Detection of buried agricultural drainage pipe with geophysical methods. *Applied Engineering in Agriculture, 20*(3), 307-318.

Annan, A. (2009). Electromagnetic principles of ground penetrating radar. *Ground penetrating radar: theory and applications. Amsterdam, The Netherlands*, 1-40.

Attia al Hagrey, S. (2007). Geophysical imaging of root-zone, trunk, and moisture heterogeneity. *Journal of Experimental Botany, 58*(4), 839-854. doi:10.1093/jxb/erl237

Born, M., & Wolf, E. (1999). *Principles of optics: electromagnetic theory of propagation, interference and diffraction of light*: Cambridge university press.

Daniels, D. J. (2004). *Ground penetrating radar* (Vol. 1): Iet.

Hillel, D. (2003). *Introduction to environmental soil physics*: Academic press.

Isselstein, J., Tallowin, J., & Smith, R. (2002). Factors affecting seed germination and seedling establishment of fen-meadow species. *Restoration Ecology, 10*(2), 173-184.

Jol, H. M. (2009). *Ground Penetrating Radar Theory and Applications*. Amsterdam, Netherlands ; Oxford, UK: Elsevier.

Ketata, M., Dhieb, M., Chaoui, M., Lahiani, M., & Ghariani, H. (2010). Electric field attenuation of an Ultra Wide Band (UWB) wave wave during propagation in the human body. *International Journal of Sciences and Techniques of Automatic Control and Computer Engineering, 4*(1), 1188 - 1197.

Kunz, K. S., & Luebbers, R. J. (1993). *The finite difference time domain method for electromagnetics*: CRC press.

Lameck, O. O., Robert, S. F., Ronald, E. Y., & Hines, J. W. (2002). *Application of Fuzzy-Neural Network in Classification of Soils using Ground-penetrating Radar Imagery*. St. Joseph, Mich. http://elibrary.asabe.org/abstract.asp?aid=11691&t=5

Mur, G. (1981). Absorbing Boundary Conditions for the Finite-Difference Approximation of the Time-Domain Electromagnetic-Field Equations. *Electromagnetic Compatibility, IEEE Transactions on, EMC-23*(4), 377-382. doi:10.1109/TEMC.1981.303970

Mur, G. (1998). Total-field absorbing boundary conditions for the time-domain electromagnetic field equations. *Electromagnetic Compatibility, IEEE Transactions on, 40*(2), 100-102.

Neal, A. (2004). Ground-penetrating radar and its use in sedimentology: principles, problems and progress. *Earth-Science Reviews, 66*(3–4), 261-330. doi:http://dx.doi.org/10.1016/j.earscirev.2004.01.004

Norimoto, M. (1976). Dielectric properties of wood.

Orfanidis, S. J. (2002). *Electromagnetic waves and antennas*: Rutgers University New Brunswick, NJ.

Sadiku, M. N. (2010). *Elements of electromagnetics* (5 ed.): Oxford university press.

Sato, M. (2009). Principles of mine detection by ground-penetrating radar *Anti-personnel Landmine Detection for Humanitarian Demining* (pp. 19-26): Springer.

Schneider, J. B. (2010). Understanding the finite-difference time-domain method. *School of electrical engineering and computer science Washington State University.–URL: http://www. Eecs. Wsu. Edu/~ schneidj/ufdtd/(request data: 29.11. 2012)*.

Topp, G., Davis, J., & Annan, A. P. (1980). Electromagnetic determination of soil water content: Measurements in coaxial transmission lines. *Water resources research, 16*(3), 574-582.

Tuller, M., & Or, D. (2004). Retention of water in soil and the soil water characteristic curve. *Encyclopedia of Soils in the Environment, 4*, 278-289.

Wang, W.-C. (1986). Electromagnetic wave theory.

Warnick, K. F. (2011). *Numerical Methods for Engineering: An Introduction Using MATLAB and Computational Electromagnetics Examples*: SciTech Pub.

Weia, J. S., & Hashimb, M. (2012). *Ground Penetrating Radar Backscatter For Underground Utility Assets Material Recognition.* Paper presented at the 33rd Asian Conference on Remote Sensing (ACRS 2012), Pattaya, Thailand.

Weiler, K. W., Steenhuis, T. S., Boll, J., & Kung, K.-J. S. (1998). Comparison of Ground Penetrating Radar and Time-Domain Reflectometry as Soil Water Sensors. *Soil Science Society of America Journal, 62*(5). doi:10.2136/sssaj1998.03615995006200050013x

Yee, K. S. (1966). Numerical solution of initial boundary value problems involving Maxwell's equations in isotropic media. *IEEE Trans. Antennas Propag, 14*(3), 302-307.

Yoder, R. E., Freeland, R. S., Ammons, J. T., & Leonard, L. L. (2001). Mapping agricultural fields with GPR and EMI to identify offsite movement of agrochemicals. *Journal of Applied Geophysics, 47*(3), 251-259.